Appl. Math. Mech. -Engl. Ed., **41**(7), 983–998 (2020)

APPLIED MATHEMATICS AND MECHANICS (ENGLISH EDITION)

https://doi.org/10.1007/s10483-020-2630-6

Research on linear/nonlinear viscous damping and hysteretic damping in nonlinear vibration isolation systems*

Zhong ZHANG[1], Muqing NIU[2,†], Kai YUAN[1], Yewei ZHANG[3]

1. Science and Technology on Reliability and Environment Engineering Laboratory, Beijing Institute of Structure and Environment Engineering, Beijing 100076, China;
2. School of Science, Harbin Institute of Technology, Shenzhen 518055, China;
3. College of Aerospace Engineering, Shenyang Aerospace University, Shenyang 110136, China

(Received Feb. 3, 2020 / Revised Apr. 9, 2020)

Abstract A nonlinear vibration isolation system is promising to provide a high-efficient broadband isolation performance. In this paper, a generalized vibration isolation system is established with nonlinear stiffness, nonlinear viscous damping, and Bouc-Wen (BW) hysteretic damping. An approximate analytical analysis is performed based on a harmonic balance method (HBM) and an alternating frequency/time (AFT) domain technique. To evaluate the damping effect, a generalized equivalent damping ratio is defined with the stiffness-varying characteristics. A comprehensive comparison of different kinds of damping is made through numerical simulations. It is found that the damping ratio of the linear damping is related to the stiffness-varying characteristics while the damping ratios of two kinds of nonlinear damping are related to the responding amplitudes. The linear damping, hysteretic damping, and nonlinear viscous damping are suitable for the small-amplitude, medium-amplitude, and large-amplitude conditions, respectively. The hysteretic damping has an extra advantage of broadband isolation.

Key words vibration isolation, nonlinear damping, Bouc-Wen (BW) model, harmonic balance method (HBM)

Chinese Library Classification O322, O328
2010 Mathematics Subject Classification 74H45

1 Introduction

Vibration reduction systems with nonlinear stiffness[1–3] allow low-frequency isolation without compromising the static stiffness, and the performance can be further improved by introducing nonlinear damping[4]. Linear damping is not efficient enough for large-amplitude vibration, and the trade-off between resonance suppression and high-frequency isolation is unavoidable.

* Citation: ZHANG, Z., NIU, M. Q., YUAN, K., and ZHANG, Y. W. Research on linear/nonlinear viscous damping and hysteretic damping in nonlinear vibration isolation systems. *Applied Mathematics and Mechanics* (*English Edition*), **41**(7), 983–998 (2020) https://doi.org/10.1007/s10483-020-2630-6

† Corresponding author, E-mail: niumuqing@hit.edu.cn

Project supported by the National Natural Science Foundation of China (No. 11902097) and the China Postdoctoral Science Foundation (No. 2019M661266)

Nonlinear damping is promising to provide a broadband high-efficient isolation performance, including nonlinear viscous damping and hysteretic damping.

Nonlinear viscous damping can be induced from viscous fluids[5], rubbers[6], and nonlinear structures[7]. The damping force is a nonlinear function of the velocity or both the velocity and the displacement. Some research[8–10] revealed that a vibration isolation system with cubic viscous damping is more effective in suppressing the resonance. More generally, Lv and Yao[11] studied a system with high-order viscous damping, and found that the nonlinear damping had a beneficial response at the resonance region while a poor performance at high frequencies. Huang et al.[12] investigated a general velocity-displacement-dependent system with nonlinear damping, and found that the displacement transmissibility in the resonance region was suppressed without affecting the transmissibility at high frequencies. Hysteretic damping can be induced from frictions[13–15], eddy current effects[16], and materials with intrinsic hysteresis[17–19], and is usually described by phenomenological models such as the bilinear model[20], the Masing model[21], and the Bouc-Wen (BW) model[22]. Barbieri et al.[23] investigated the nonlinear dynamic behavior of a wire rope isolator and an asymmetric Stockbridge damper, and verified that the BW model was well suited for hysteretic damping systems. Carboni and Lacarbonara[24] established a modified BW model to represent the pinched hysteresis derived from mixed wire ropes made of nitinol and steel.

In most studies, nonlinear viscous damping and hysteretic damping are investigated separately, while the comparative research on different kinds of damping is limited. Solovyov et al.[25] compared linear damping, nonlinear viscous damping, and BW hysteretic damping, and pointed out that hysteretic damping was highly efficient both in and out of the resonance region. However, the study is limited to the isolation system with linear stiffness. For BW hysteresis, both the stiffness softening effect and the damping effect contribute to the isolation performance. It is more reasonable to separate the two effects and focus only on the damping effect. Equivalent damping ratio is mostly used to evaluate the damping effect of nonlinear damping, and is calculated through the dissipated energy and the elastic energy. For nonlinear stiffness systems, the elastic energy is usually calculated through the initial stiffness or the average stiffness[26]. It is inaccurate for the systems with strong nonlinearities, and the influence of hysteretic damping on the stiffness is not considered.

The dynamic systems with strong nonlinearities are difficult to be analyzed analytically. The promising methods include the harmonic balance method (HBM)[27], the hyperbolic perturbation method[28], and the averaging method[29–30]. The inclusion of hysteretic damping makes the analysis more challenging, because damping forces are mainly non-smooth and expressed by piecewise or implicit functions. Xiong et al.[31] and Wu et al.[32] adopted the increment HBM to determine the periodic solutions of bilinear hysteretic systems. Wong et al.[33] treated a BW hysteretic system with an analytical-numerical method based on the HBM and a Levenberg-Marquardt (LM) algorithm. The alternating frequency/time (AFT) domain technique[34–35] is practical to deal with the nonlinear functions. However, the solution of dynamic equations with both nonlinear explicit and implicit functions is still challenging.

In this paper, a generalized vibration isolation system is established with nonlinear stiffness expressed by a polynomial function of the displacement, nonlinear viscous damping expressed by a polynomial function of the velocity, and hysteretic damping expressed by an implicit function of the BW model. The approximate analytical solution of the model is acquired through an HBM-AFT-LM method. An analytical recursive method is proposed for the polynomial functions, and the implicit function is dealt with a numerical AFT method. A generalized equivalent damping ratio is defined with the stiffness-varying characteristics. The basic characteristics of different kinds of damping are revealed, and a comprehensive comparison of the damping effects is carried out. The remainder of this paper is organized as follows. The generalized vibration isolation model and the approximate analytical solution are presented in Section 2. The generalized equivalent damping ratio is defined in Section 3. The numerical simulation and discussion

are demonstrated in Section 4. Conclusions are drawn in Section 5.

2 Modeling and approximate analytical solution

Consider a generalized vibration isolation system shown in Fig. 1. The payload mass is denoted as M. The elastic component presents a restoring force expressed by a polynomial function with the ith-order ($i = 1, 2, \cdots, n_{\mathrm{k}}$) stiffness K_i. The viscous damping component presents a damping force expressed by a polynomial function with the ith-order ($i = 1, 2, \cdots, n_{\mathrm{c}}$) damping C_i. The stiffness and viscous damping can be linear or nonlinear, depending on the high-order coefficients. The hysteretic damping force is denoted as Z. Under the initial condition, the system is statically balanced and $Z = 0$ (no residual hysteretic force). A harmonic excitation is applied on the base with the displacement expressed as $X_{\mathrm{e}} = A_{\mathrm{e}} \cos(\omega_{\mathrm{e}} T)$, where A_{e}, ω_{e}, and T denote the amplitude, the frequency, and the time, respectively. The responding displacement of the payload is denoted as X_{p}. The relative displacement is denoted as $X = X_{\mathrm{p}} - X_{\mathrm{e}}$.

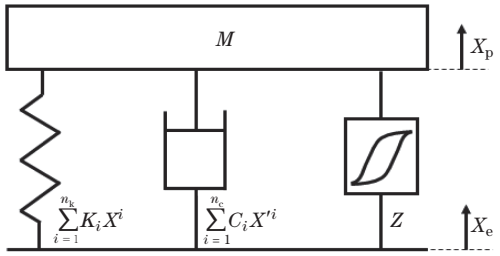

Fig. 1 A generalized vibration isolation system

The dynamic equation of the system is

$$MX'' + \sum_{i=1}^{n_{\mathrm{k}}} K_i X^i + \sum_{i=1}^{n_{\mathrm{c}}} C_i X'^i + Z = M A_{\mathrm{e}} \omega_{\mathrm{e}}^2 \cos(\omega_{\mathrm{e}} T). \tag{1}$$

The hysteretic damping force is described with a BW model as follows[22]:

$$Z' = (K_{\mathrm{d}} - (\gamma + \beta \operatorname{sgn}(X'Z))|Z|^{n_{\mathrm{bw}}})X', \tag{2}$$

where K_{d}, γ, β, and n_{bw} are the BW model parameters. The introduction of dimensionless parameters transforms Eqs. (1) and (2) into

$$\eta^2 \ddot{x} + \sum_{i=1}^{n_{\mathrm{k}}} k_i x^i + \sum_{i=1}^{n_{\mathrm{c}}} c_i (\eta \dot{x})^i + \frac{1 - k_1}{\rho} z = \eta^2 a_{\mathrm{e}} \cos t, \tag{3}$$

$$\dot{z} = (1 - (1 - \sigma + \sigma \operatorname{sgn}(\dot{x} z))|z|^{n_{\mathrm{bw}}})\rho \dot{x}, \tag{4}$$

where

$$\begin{cases} \omega_{\mathrm{c}} = \sqrt{\dfrac{K_1 + K_{\mathrm{d}}}{M}}, \quad t = \omega_{\mathrm{e}} T, \quad k_i = \dfrac{K_i X_{\mathrm{c}}^{i-1}}{K_1 + K_{\mathrm{d}}}, \\ c_i = \dfrac{C_i X_{\mathrm{c}}^{i-1} \omega_{\mathrm{c}}^i}{K_1 + K_{\mathrm{d}}}, \quad x = \dfrac{X}{X_{\mathrm{c}}}, \quad z = \dfrac{Z}{K_{\mathrm{d}} X_{\mathrm{c}}}, \\ \rho = \left((\gamma + \beta) K_{\mathrm{d}}^{n_{\mathrm{bw}} - 1} X_{\mathrm{c}}^{n_{\mathrm{bw}}}\right)^{\frac{1}{n_{\mathrm{bw}}}}, \quad \sigma = \dfrac{\beta}{\gamma + \beta}, \quad a_{\mathrm{e}} = \dfrac{A_{\mathrm{e}}}{X_{\mathrm{c}}}, \quad \eta = \dfrac{\omega_{\mathrm{e}}}{\omega_{\mathrm{c}}}. \end{cases} \tag{5}$$

In the above equations, ω_{c} and X_{c} are the characteristic frequency and displacement, respectively. The dimensionless initial stiffness of the system is 1. In order to study the shape of the BW hysteresis loop, the dimensionless hysteretic force z is normalized with the maximum limit value of 1. When $n \to \infty$, the BW hysteresis becomes bilinear. A necessary and sufficient condition for the thermodynamic admissibility of the BW hysteresis is $-\beta \leqslant \gamma \leqslant \beta$[36]. Thus, we focus on the parameter domain of $\rho > 0$ and $\sigma \geqslant 0.5$, where the hysteresis presents a stiffness softening behavior. The stiffness of the system mainly depends on k_i, ρ, and n_{bw}. The change of σ has little influence on the stiffness, which is the basis for the separation of the stiffness softening effect and the damping effect of the BW hysteresis in this research.

The approximate analytical solution of Eqs. (3) and (4) is based on an HBM-AFT-LM method. Assume the following Fourier expansions:

$$x = a_0 + \sum_{i=1}^{m} (a_i \cos(it) + b_i \sin(it)), \tag{6}$$

$$x^j = p_0^{(j)} + \sum_{i=1}^{m} (p_i^{(j)} \cos(it) + q_i^{(j)} \sin(it)), \tag{7}$$

where m is the selected harmonic order and $m \geqslant \max(n_{\mathrm{k}}, n_{\mathrm{c}})$. The harmonic coefficients of high-order displacement terms can be calculated with a recursive method as follows:

$$p_0^{(j)} = \frac{1}{2} \sum_{l=1}^{m} (p_l^{(j-1)} a_l + q_l^{(j-1)} b_l) + p_0^{(j-1)} a_0, \tag{8}$$

$$\begin{aligned} p_i^{(j)} = \frac{1}{2} (& \sum_{l=0}^{m-i} p_l^{(j-1)} a_{l+i} + \sum_{l=i}^{m} p_l^{(j-1)} a_{l-i} + \sum_{l=0}^{i} p_l^{(j-1)} a_{i-l} + \sum_{l=1}^{m-i} q_l^{(j-1)} b_{l+i} \\ & + \sum_{l=i+1}^{m} q_l^{(j-1)} b_{l-i} - \sum_{l=1}^{i-1} q_l^{(j-1)} b_{i-l}), \end{aligned} \tag{9}$$

$$\begin{aligned} q_i^{(j)} = \frac{1}{2} (& \sum_{l=0}^{m-i} p_l^{(j-1)} b_{l+i} + \sum_{l=i}^{m} q_l^{(j-1)} a_{l-i} - \sum_{l=1}^{m-i} q_l^{(j-1)} a_{l+i} - \sum_{l=i+1}^{m} p_l^{(j-1)} b_{l-i} \\ & + \sum_{l=0}^{i-1} p_l^{(j-1)} b_{i-l} + \sum_{l=1}^{i} q_l^{(j-1)} a_{i-l}). \end{aligned} \tag{10}$$

The Fourier expansion of the velocity term is expressed as follows:

$$\dot{x} = \sum_{i=1}^{m} (i b_i \cos(it) - i a_i \sin(it)). \tag{11}$$

The harmonic coefficients of high-order velocity terms can be acquired in a similar way to Eqs. (8)–(10) by replacing a_l and b_l with $l b_l$ and $-l a_l$, respectively. The Fourier expansion of z is expressed as follows:

$$z = c_0 + \sum_{i=1}^{m} (c_i \cos(it) + d_i \sin(it)), \tag{12}$$

where c_0, c_i, and d_i are harmonic coefficients and can be obtained through the harmonic balance process based on Eq. (3). According to Eq. (4), the residual r is defined as follows:

$$r = \dot{z} - (1 - (1 - \sigma + \sigma \operatorname{sgn}(\dot{x} z)) |z|^{n_{\mathrm{bw}}}) \rho \dot{x}, \tag{13}$$

which is a multi-valued and non-smooth function. An AFT technique is adopted to acquire the corresponding harmonic coefficients. Define a discrete time sequence from $t = 0$ to $t = 2\pi$, whose length is one period for the dimensionless time. The discrete sequences of $x^i(t)$, $\dot{x}^i(t)$, $z(t)$, and $\dot{z}(t)$ can be acquired based on their Fourier expansions. The discrete sequence of $r(t)$ is calculated according to Eq. (13). The harmonic coefficients of r can be numerically obtained through a fast Fourier transform as follows:

$$r = u_0 + \sum_{i=1}^{m} (u_i \cos(it) + v_i \sin(it)). \tag{14}$$

Define

$$\begin{cases} \boldsymbol{A} = (a_0, a_1, \cdots, a_m, b_1, \cdots, b_m)^{\mathrm{T}}, \\ \boldsymbol{U} = (u_0, u_1, \cdots, u_m, v_1, \cdots, v_m)^{\mathrm{T}}. \end{cases}$$

It is obvious that $\boldsymbol{U}$ is a function of $\boldsymbol{A}$. Through the HBM and AFT, solving the differential equations (3) and (4) is equivalent to the least-square problem of searching $\boldsymbol{A}$ to achieve the minimum value of $\boldsymbol{U}^{\mathrm{T}}\boldsymbol{U}$. An LM algorithm is adopted to seek the least-square solution with the iteration formula of Ref. [33] as follows:

$$\boldsymbol{A}^{(w+1)} = \boldsymbol{A}^{(w)} - \left(\boldsymbol{J}^{\mathrm{T}}_{[\boldsymbol{A}^{(w)}]}\boldsymbol{J}_{[\boldsymbol{A}^{(w)}]} + \phi^{(w)}\boldsymbol{I}\right)^{-1}\boldsymbol{J}^{\mathrm{T}}_{[\boldsymbol{A}^{(w)}]}\boldsymbol{U}_{[\boldsymbol{A}^{(w)}]}, \tag{15}$$

where the superscript denotes the number of iterations, and ϕ is an LM parameter. $\boldsymbol{I}$ is the identity matrix. $\boldsymbol{J}$ is the Jacobi matrix of $\boldsymbol{U}$ expressed by

$$\boldsymbol{J} = \Big(\frac{\partial \boldsymbol{U}}{\partial a_0}, \frac{\partial \boldsymbol{U}}{\partial a_1}, \cdots, \frac{\partial \boldsymbol{U}}{\partial a_m}, \frac{\partial \boldsymbol{U}}{\partial b_1}, \cdots, \frac{\partial \boldsymbol{U}}{\partial b_m}\Big).$$

Each column of $\boldsymbol{J}$ can be calculated through the AFT technique. For example, consider the following discrete sequence in the time domain:

$$\begin{aligned} \frac{\partial r(t)}{\partial a_i} &= \frac{\partial r(t)}{\partial \dot{x}}\frac{\partial \dot{x}}{\partial a_i} + \frac{\partial r(t)}{\partial z}\frac{\partial z}{\partial a_i} + \frac{\partial r(t)}{\partial \dot{z}}\frac{\partial \dot{z}}{\partial a_i} \\ &= \rho((1-\sigma+\sigma\,\mathrm{sgn}(\dot{x}(t)z(t)))|z(t)|^{n_{\mathrm{bw}}}-1)\frac{\partial \dot{x}}{\partial a_i} \\ &\quad + \rho\dot{x}(t)n_{\mathrm{bw}}((1-\sigma)\mathrm{sgn}(z(t)) + \sigma\,\mathrm{sgn}(\dot{x}(t)))|z(t)|^{n_{\mathrm{bw}}-1}\frac{\partial z}{\partial a_i} + \frac{\partial \dot{z}}{\partial a_i}, \end{aligned} \tag{16}$$

where $\frac{\partial \dot{x}}{\partial a_i}$, $\frac{\partial z}{\partial a_i}$, and $\frac{\partial \dot{z}}{\partial a_i}$ can be calculated analytically. The harmonic coefficients of $\frac{\partial r(t)}{\partial a_i}$ can be obtained through a fast Fourier transform, which are the elements of $\frac{\partial \boldsymbol{U}}{\partial a_i}$ in $\boldsymbol{J}$. By iterations, the solution of $\boldsymbol{A}$ is obtained when the least-square error of $\boldsymbol{U}$ is below a determined tolerance, and then the solution of x is acquired.

In conclusion, the approximate analytical analysis is based on the HBM. The Fourier expansions and related partial derivatives of the high-order terms are calculated with the recursive method. The BW hysteretic terms are dealt with the AFT. The nonlinear algebra equations are solved by iterations based on the LM algorithm. The frequency responses can be obtained through a swept frequency (changing η) process. The flow chart of the approximate analytical method is presented in Fig. 2.

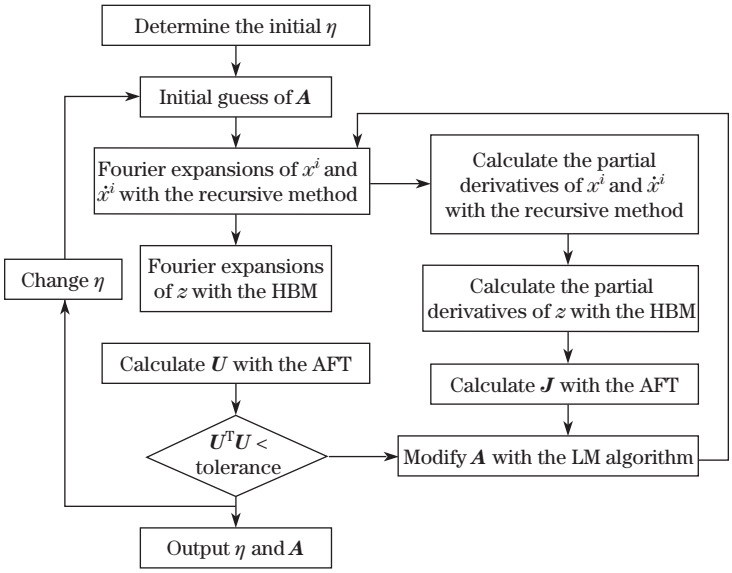

Fig. 2 Flow chart of the approximate analytical method

3 Generalized equivalent damping ratio

A generalized equivalent damping ratio is defined to evaluate the damping effect. The steady state response of the system is periodic. The dimensionless restoring force of the isolation system is expressed as follows:

$$f = \sum_{i=1}^{n_{\mathrm{k}}} k_i x^i + \sum_{i=1}^{n_{\mathrm{c}}} c_i (\eta\dot{x})^i + \frac{1-k_1}{\rho} z. \tag{17}$$

The dimensionless energy dissipation per cycle equals the area of the hysteresis loop, i.e.,

$$E_{\mathrm{d}} = \int_{-a}^{a} f \mathrm{d}x - \int_{a}^{-a} f \mathrm{d}x, \tag{18}$$

where a is the amplitude of x. With the increase in σ, the area of the hysteresis loop increases, while the stiffness-varying behavior is not affected. The BW function of Eq. (4) becomes a single-valued function when $\sigma = 0$. Thus, an anhysteretic BW force z_{an} can be defined by

$$\dot{z}_{\mathrm{an}} = (1 - |z|^{n_{\mathrm{bw}}})\rho\dot{x}. \tag{19}$$

Then, the anhysteretic restoring force is expressed as

$$f_{\mathrm{an}} = \sum_{i=1}^{n_{\mathrm{k}}} k_i x^i + \frac{1-k_1}{\rho} z_{\mathrm{an}}. \tag{20}$$

The anhysteretic restoring force is a single-valued (undamped) function, which characterizes the stiffness-varying behavior induced from the high-order stiffness and the BW model. It can be regarded as a generalized frequency-independent elastic restoring force. The maximum generalized elastic energy can be calculated as follows:

$$E_{\mathrm{e}} = \int_{0}^{a} f_{\mathrm{an}} \mathrm{d}x. \tag{21}$$

The generalized equivalent damping ratio is defined by

$$\zeta = \frac{E_{\mathrm{d}}}{4\pi\eta E_{\mathrm{e}}}. \tag{22}$$

Compared with the equivalent damping ratio calculated with the initial stiffness or the average stiffness, the proposed generalized equivalent damping ratio is more accurate in evaluating the elastic energy. Obviously, for the systems with monotonically varying stiffness, the calculated damping ratio is between the results calculated with the initial stiffness and the average stiffness. Besides, the stiffness-softening effect is separated from the damping effect of the BW hysteresis, and it is considered in the generalized elastic energy. The comparisons among the linear viscous damping, the nonlinear viscous damping, and the BW hysteretic damping without the stiffness change influence become available.

4 Simulation and discussion

4.1 Basic characteristics

The basic characteristics of the linear and nonlinear viscous damping are studied by calculating their generalized equivalent damping ratios in different systems. Consider the following isolation system model:

$$\eta^2\ddot{x} + k_1 x + k_3 x^3 + c_1\dot{x} + c_3\eta^3\dot{x}^3 = \eta^2 a_{\mathrm{e}}\cos t, \tag{23}$$

where $k_1 = 1$, $c_1 = 0.4$, and $a_{\mathrm{e}} = 1$. The cubic stiffness coefficient is $k_3 = 0$, 0.05 and –0.05, corresponding to linear stiffness, stiffness hardening, and stiffness softening systems, respectively. The cubic damping coefficient is $c_3 = 0$ and 0.01, corresponding to linear and nonlinear viscous damping, respectively. Only odd-order stiffness and damping are considered to avoid the deviation of dynamic equilibrium location ($a_0 = 0$). The dimensionless displacement response of the payload is denoted as $x_{\mathrm{p}} = x + x_{\mathrm{e}}$, and its amplitude is denoted as a_{p}.

The amplitude-frequency responses are shown in Fig. 3(a). With the same damping coefficient, the stiffness softening system shows a better isolation performance than the linear system, while the stiffness hardening system shows a worse isolation performance than the linear system. The additional high-order damping enhances the isolation performance regardless of the stiffness variation. The generalized equivalent damping ratios are shown in Fig. 3(b). With linear viscous damping, the damping ratio is a constant for the linear system. For the stiffness hardening system, the damping ratio decreases with the increase in the stiffness, and reaches the minimum at the resonance. The lower damping ratio illustrates the worse isolation performance of the stiffness hardening system. The trend is opposite for the stiffness softening system. The additional high-order damping increases the damping ratio, especially at the resonant region.

The basic characteristics of the BW hysteretic damping are studied through the hysteresis loop and the damping ratio. Assume that x is harmonic with the dimensionless frequency of $\eta = \pi/4$. The normalized hysteretic force z is calculated through Eq. (4), where $\rho = 1$, $\sigma = 0$, 0.5, and 1, and $n_{\mathrm{bw}} = 1$ and 5. When the amplitude is $a = 5$, the normalized hysteresis loops are shown in Fig. 4(a). When $\sigma = 0$, the single-valued curves correspond to the anhysteretic BW forces expressed in Eq. (19). With the increase in σ, the area of the hysteresis loop increases. With the increase in n_{bw}, the loop becomes sharper and tends to bilinear hysteresis. The generalized equivalent damping ratio is calculated when $k_1 = 0.2$ and there is no viscous damping. Obviously, $\zeta = 0$ when $\sigma = 0$. The calculation results with $\sigma > 0$ are shown in Fig. 4(b), which are related to the amplitude. The damping ratio first increases, and then decreases. The amplitude with the maximum damping ratio is the 'best amplitude for the BW hysteretic damping', which is denoted as a_{bw}. When σ increases, the damping ratio increases. When n_{bw} increases, the damping ratio changes more dramatically.

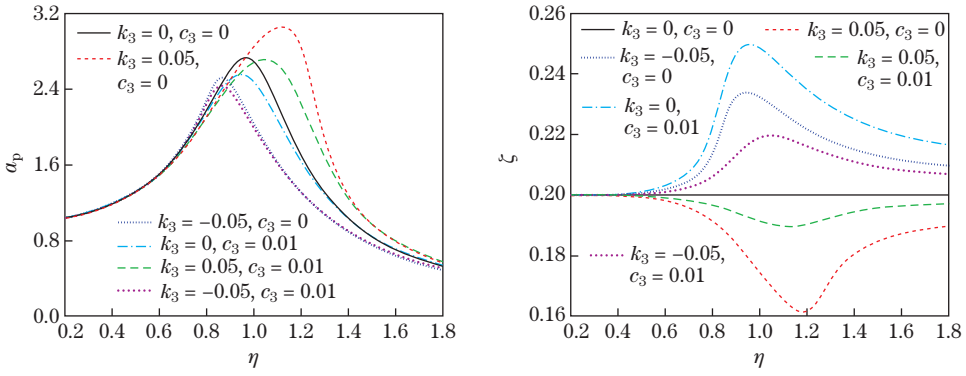

(a) Amplitude-frequency response (b) Generalized equivalent damping ratio

Fig. 3 Basic characteristics of linear and nonlinear viscous damping (color online)

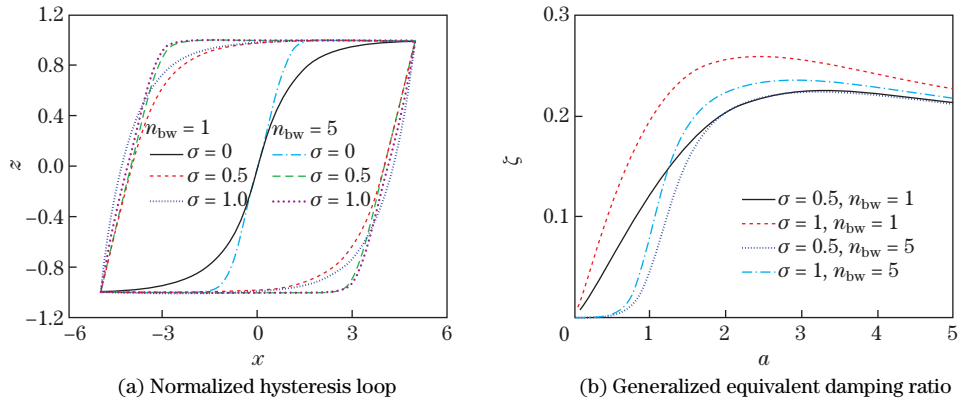

(a) Normalized hysteresis loop (b) Generalized equivalent damping ratio

Fig. 4 Basic characteristics of the BW hysteretic damping (color online)

Consider the following system:

$$\eta^2\ddot{x} + \sum_{i=1}^{n_k} k_i x^i + \sum_{i=1}^{n_c} c_i(\eta\dot{x})^i + \frac{1-k_1}{\rho} z_{an} = \eta^2 a_e \cos t, \tag{24}$$

where z_{an} is expressed in Eq. (19). The stiffness-varying characteristics of the system are the same as those of Eq. (3). Thus, the comparison between the viscous damping and the hysteretic damping is available. The determined parameters include $k_1 = 0.5$, $k_3 = 5\times10^{-3}$, $k_5 = 5\times10^{-4}$, and $\rho = 1$. The excitation amplitudes are selected as $a_e = 0.4$, 0.7, 1, 1.3, 1.6. Four groups of damping are studied (see Table 1). Although the change of n_{bw} affects the stiffness-varying behavior, it is still studied because it is a key parameter for the shape of the hysteresis loop.

Table 1 Coefficients of four groups of damping

Group	c_1	c_3	σ	n_{bw}
A	0.4	0	0	1
B	0.32	0.01	0	1
C	0.2	0	1	1
D	0.2	0	1	5

The amplitude-frequency responses and generalized equivalent damping ratios of four groups of damping are shown in Figs. 5 and 6. The system presents a stiffness softening-hardening behavior with a boundary amplitude a_{sh}. The response of the payload becomes larger when the excitation amplitude increases. For Group A, the damping is linear. The boundary amplitudes for the stiffness-softening and stiffness-hardening regions are $a_{\mathrm{sh}} = 3.03$. In the stiffness softening region ($a < a_{\mathrm{sh}}$), the damping ratio increases when the amplitude increases. While in the stiffness hardening region ($a > a_{\mathrm{sh}}$), the damping ratio decreases when the amplitude increases, which leads to the 'valley phenomenon' at the resonant region when $a_{\mathrm{e}} = 1.6$ (see Fig. 5(b)). For Group B, part of the linear damping is replaced by cubic damping. The damping ratio decreases when the amplitude is low. When $a_{\mathrm{e}} = 0.4$, the damping ratio in Fig. 5(d) is smaller than that in Fig. 5(b) at all frequencies. The damping ratio increases when the amplitude is high, and the 'valley phenomenon' does not occur. For Group C, a combination of linear damping and hysteretic damping is studied. The amplitude corresponding to the maximum damping ratio is $a_{\mathrm{bw}} = 1.76$. The damping ratio increases dramatically with the amplitude when $a < a_{\mathrm{bw}}$, and decreases when $a > a_{\mathrm{bw}}$. The 'valley phenomenon' can be spotted when $a_{\mathrm{e}} = 1.3$ and 1.6 (see Fig. 6(b)). However, the cause is totally different from that under the linear damping condition. For the hysteretic damping, the decrease in the damping ratio is related to the responding amplitude rather than the stiffness-varying characteristics. An obvious proof can be found in Fig. 6(b). The damping ratio decreases when $a_{\mathrm{bw}} < a < a_{\mathrm{sh}}$, which is in the stiffness softening region. For Group D, with the increase in n_{bw}, the damping ratio increases and decreases more dramatically. The amplitude corresponding to the maximum damping ratio is $a_{\mathrm{bw}} = 2.16$. The amplitude band in which the hysteretic damping is effective becomes narrower.

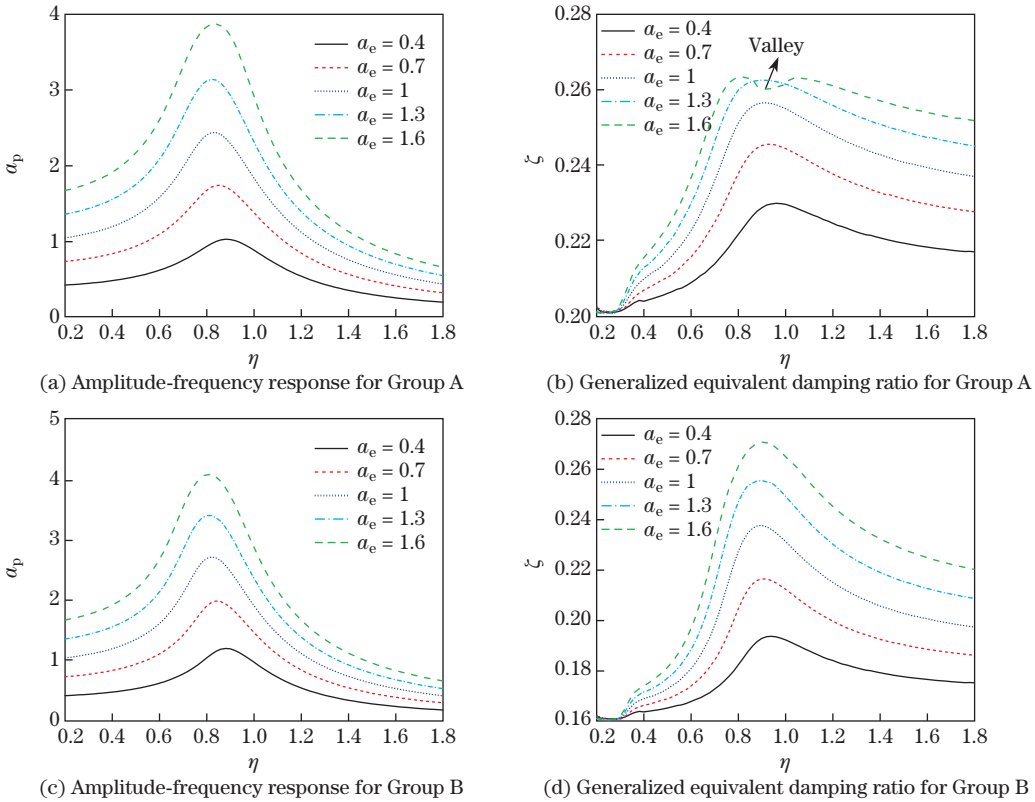

(a) Amplitude-frequency response for Group A

(b) Generalized equivalent damping ratio for Group A

(c) Amplitude-frequency response for Group B

(d) Generalized equivalent damping ratio for Group B

Fig. 5 Amplitude-frequency responses and damping ratios of Groups A and B (color online)

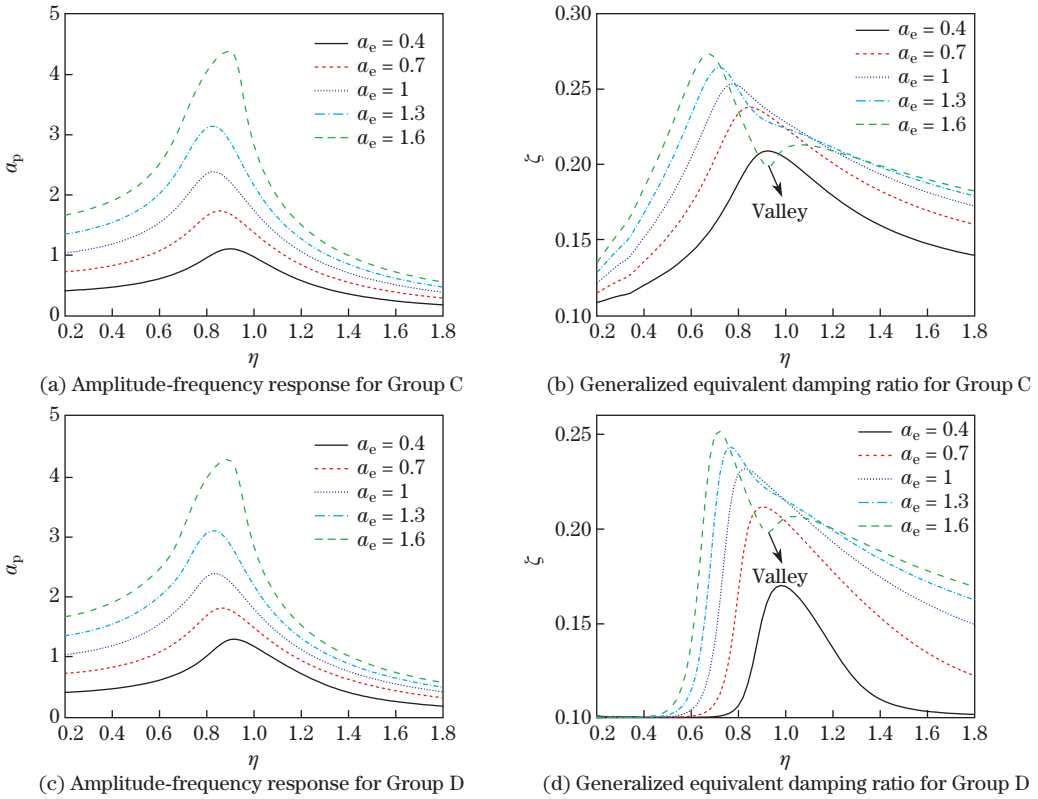

(a) Amplitude-frequency response for Group C

(b) Generalized equivalent damping ratio for Group C

(c) Amplitude-frequency response for Group D

(d) Generalized equivalent damping ratio for Group D

Fig. 6 Amplitude-frequency responses and damping ratios of Groups C and D (color online)

4.2 Comparison of the damping effects

The dissipated energy (the area of the hysteresis loop) of each kind of damping can be adjusted by their control parameters. It is hard to compare the damping effect of different damping forms without a uniform standard. In this research, the stiffness-varying characteristics and the dissipated energy are the same for the systems with different damping forms. Therefore, the damping effect difference only lies in the intrinsic property of damping (the shape of the hysteresis loop). Some cases are studied according to this rule.

Case 1 The determined parameters are

$$\begin{cases} k_1 = 0.5, \quad k_3 = 5 \times 10^{-3}, \quad k_5 = 5 \times 10^{-4}, \\ \rho = 1, \quad n_{\mathrm{bw}} = 1, \quad a_{\mathrm{e}} = 1.6, \quad \eta = 0.9. \end{cases}$$

The damping coefficients and calculated damping effects are shown in Table 2. Under this condition, Group B with cubic damping presents the largest damping ratio and the smallest payload amplitude. The linear damping and the hysteretic damping are unable to provide such effects because of the 'valley phenomena'. For the stiffness softening system, the 'valley phenomenon' does not occur for linear damping. However, high-order damping is still more effective for larger amplitude. The damping ratio only reflects the overall damping effect. It is noted that the amplitude of the 3rd harmonics (denoted as $(a_3^2 + b_3^2)^{1/2}$) in Group A is much smaller than those in Groups B and C. The hysteresis loops are shown in Fig. 7. The areas of the loops are the same. The widest loop of Group B represents the best damping performance.

Table 2 Damping coefficients and calculated damping effects of Case 1

Group	c_1	c_3	σ	E_d	ζ	a_p	$(a_1^2+b_1^2)^{1/2}$	$(a_3^2+b_3^2)^{1/2}$	$(a_5^2+b_5^2)^{1/2}$
A	0.4	0	0	14.35	0.26	3.70	3.56	2.86×10^{-3}	3.65×10^{-3}
B	0.246	0.03	0	14.35	0.32	3.35	3.24	2.85×10^{-2}	2.20×10^{-3}
C	0.252	0	0.5	14.34	0.24	3.59	3.64	4.13×10^{-2}	2.00×10^{-3}

Case 2 The determined parameters are

$$\begin{cases} k_1 = 0.5, \quad k_3 = 0.01, \quad k_5 = 5\times10^{-4}, \\ \rho = 1, \quad n_\mathrm{bw} = 1, \quad a_\mathrm{e} = 1, \quad \eta = 0.78. \end{cases}$$

The damping coefficients and calculated damping effects are shown in Table 3, and the hysteresis loops are shown in Fig. 8. Under this condition, the amplitude of the relative displacement is close to a_bw. Thus, Group C with BW hysteretic damping presents the best overall damping effect. However, the amplitude of the 3rd harmonics is about twice of those of Groups A and B.

Table 3 Damping coefficients and calculated damping effects of Case 2

Group	c_1	c_3	σ	E_d	ζ	a_p	$(a_1^2+b_1^2)^{1/2}$	$(a_3^2+b_3^2)^{1/2}$	$(a_5^2+b_5^2)^{1/2}$
A	0.4	0	0	2.75	0.25	2.34	1.67	8.86×10^{-3}	1.11×10^{-3}
B	0.399	0.01	0	2.75	0.26	2.30	1.63	8.77×10^{-3}	1.05×10^{-3}
C	0.252	0	2	2.75	0.27	2.17	1.57	1.61×10^{-2}	1.66×10^{-3}

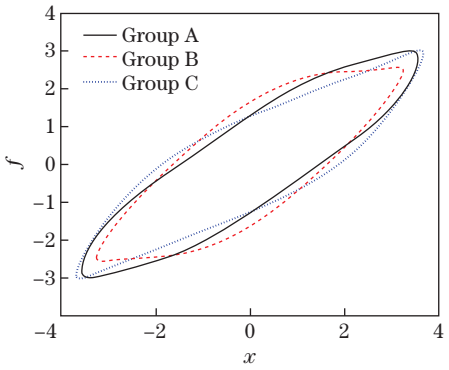

Fig. 7 Hysteresis loops of Case 1 (color online)

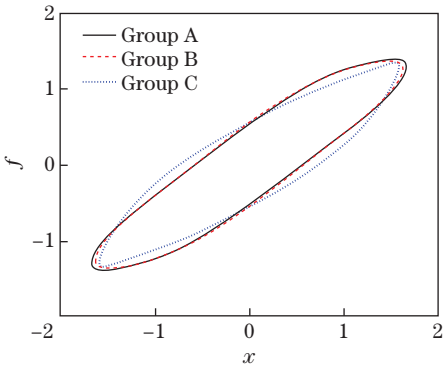

Fig. 8 Hysteresis loops of Case 2 (color online)

Case 3 The determined parameters are

$$\begin{cases} k_1 = 0.5, \quad k_3 = 5\times10^{-3}, \quad k_5 = 5\times10^{-4}, \\ \rho = 1, \quad n_\mathrm{bw} = 1, \quad a_\mathrm{e} = 0.4, \quad \eta = 0.96. \end{cases}$$

The damping coefficients and the calculated damping effects are shown in Table 4, and the hysteresis loops are shown in Fig. 9. Under this small-amplitude condition, the high-order damping has few effects. The hysteresis loop shapes of Groups A and B are almost the same. Group C with the hysteretic damping presents a different hysteresis loop shape. However, the damping ratio is approximately the same as that of Group A, and a_p is larger. For simplicity, linear damping is more preferred for small amplitude conditions.

Table 4 Damping coefficients and calculated damping effects of Case 3

Group	c_1	c_3	σ	E_d	ζ	a_p	$(a_1^2+b_1^2)^{1/2}$	$(a_3^2+b_3^2)^{1/2}$	$(a_5^2+b_5^2)^{1/2}$
A	0.4	0	0	1.07	0.23	0.952	0.942	3.06×10^{-3}	2.43×10^{-4}
B	0.383	0.03	0	1.07	0.23	0.949	0.938	3.13×10^{-3}	2.38×10^{-4}
C	0.186	0	2	1.07	0.23	0.966	0.933	5.35×10^{-3}	6.22×10^{-4}

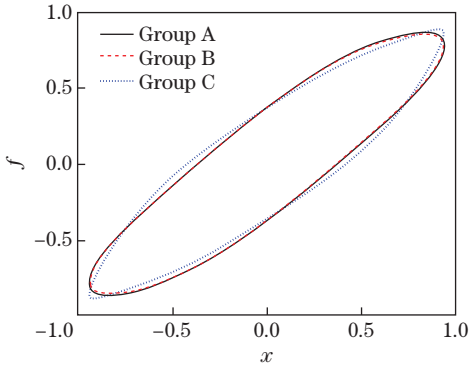

Fig. 9 Hysteresis loops of Case 3 (color online)

It can be concluded from the harmonic excitation simulations that the relationship of linear damping, high-order damping, and hysteretic damping is complicated. It depends on the stiffness-varying characteristics, the excitation amplitude, and the frequency. A qualitative conclusion can be made that high-order damping, hysteretic damping, and linear damping are more effective for large, medium, and small response amplitudes, respectively.

In order to study the damping effects at high frequencies, a swept-frequency simulation is performed. The determined parameters are

$$\begin{cases} k_1 = 0.5, \quad k_3 = 5\times10^{-3}, \quad k_5 = 5\times10^{-4}, \\ \rho = 1, \quad n_\mathrm{bw} = 1, \quad a_\mathrm{e} = 1.6. \end{cases}$$

Three groups of damping are studied with the coefficients as follows:

$$\text{Group A:} \quad c_1 = 0.4, \quad c_3 = \sigma = 0;$$

$$\text{Group B:} \quad c_1 = 0.266, \quad c_3 = 0.03, \quad \sigma = 0;$$

$$\text{Group C:} \quad c_1 = 0.207, \quad c_3 = 0, \quad \sigma = 2.$$

The amplitude-frequency responses of the payload amplitude (a_p) and the coefficients of the 1st-order harmonics (a_1 and b_1) are shown in Fig. 10. It can be seen from Fig. 10(a) that the maximum amplitudes of Groups A, B, and C are 3.87. Thus, the damping effect can be compared with a uniform standard. At high frequencies where the vibration is effectively isolated, Group C with the BW hysteretic damping presents the best isolation performance, while Group B with high-order damping presents the worst. It is further demonstrated in Fig. 10(b) that the main difference lies in the 1st-order sine coefficient (b_1). The high-frequency isolation performance mainly depends on the phase rather than the equivalent damping ratio. Besides, with smaller excitation amplitude, the BW hysteretic damping still presents the best high-frequency isolation performance.

For the same system, in which $a_\mathrm{e} = 1$, the effects of different damping coefficients on the broadband isolation performance are studied, and the results are shown in Fig. 11.

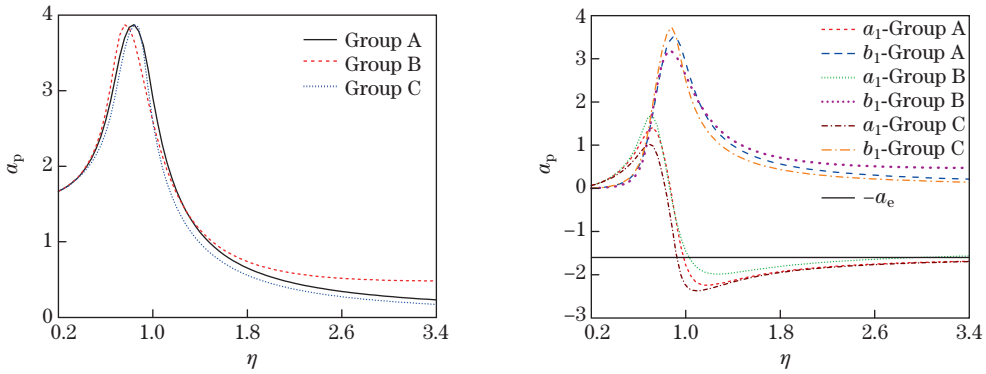

(a) Payload amplitude (b) Coefficients of the 1st-order harmonics

Fig. 10 Amplitude-frequency responses of the payload amplitude and coefficients of the 1st-order harmonics (color online)

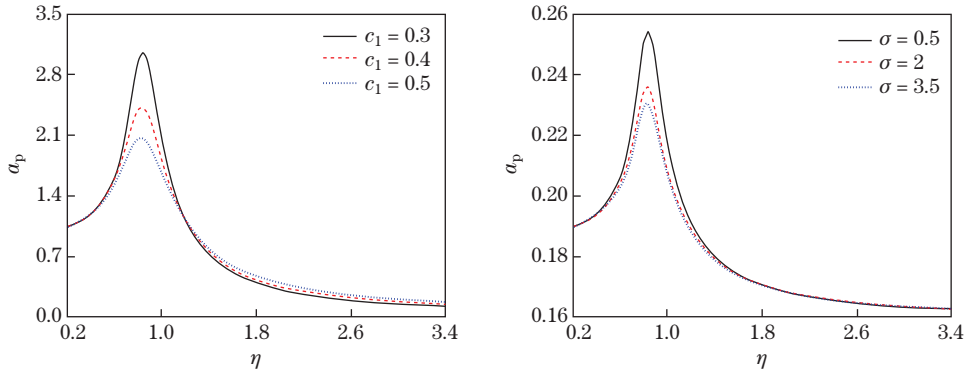

(a) Different linear damping coefficients (b) Different hysteretic damping coefficients

Fig. 11 Amplitude-frequency responses with different linear damping and hysteretic damping coefficients (color online)

In Fig. 11(a), only linear damping is considered. when the linear damping coefficient increases, the resonance is more effectively suppressed while the high-frequency isolation becomes worse. In Fig. 11(b), the linear damping coefficient of $c_1 = 0.12$ is fixed. When the hysteretic damping coefficient increases, the resonance is more effectively suppressed without affecting the high-frequency isolation performance. From this point of view, the BW hysteretic damping is also more preferred for broadband isolation.

5 Conclusions

This research makes a comprehensive study on linear damping, nonlinear viscous damping, and BW hysteretic damping. A generalized nonlinear vibration isolation model is established and analytically solved with an HBM-AFT-LM method. A generalized equivalent damping ratio is defined with the stiffness-varying characteristics counted in the elastic energy. The separation of the stiffness softening effect and the damping effect of the BW hysteresis is the basis for the comparison of different damping forms. Conclusions are drawn for the characteristics and suitable ranges of three kinds of damping.

Linear damping is the most basic damping form. The damping ratio increases with stiffness

softening while decreases with stiffness hardening. For the stiffness softening-hardening system with the boundary amplitude of $a_{\rm sh}$, a 'valley phenomenon' occurs when the amplitude exceeds $a_{\rm sh}$. Linear damping applies to small-amplitude conditions.

High-order damping is a typical kind of nonlinear viscous damping. The damping ratio increases with the amplitude regardless of the stiffness-varying characteristics. High-order damping is the most effective under large-amplitude conditions. However, it may deteriorate a high-frequency isolation performance.

BW hysteretic damping is a typical non-viscous damping. With the increase in the amplitude, the damping ratio first increases dramatically, and then decreases. With the increase in $n_{\rm bw}$, the damping ratio tends to be like bilinear hysteresis, and its increase and decrease are more dramatic. The damping ratio reaches the maximum at $a = a_{\rm bw}$, and a 'valley phenomenon' occurs when the amplitude exceeds this value. BW hysteretic damping is most effective when the amplitude is around $a_{\rm bw}$. A unique advantage for BW hysteretic damping is that it has little influence on the high-frequency isolation performance.

Different damping forms lead to different shapes of hysteresis loops. Even with the same loop area, i.e., the same dissipated energy, the damping effects are different. The best choice of damping forms depends on the stiffness-varying characteristics of the isolation system, the required frequency band, and the excitation amplitude.

References

[1] LU, Z. Q., YANG, T. J., BRENNAN, M. J., LIU, Z. G., and CHEN, L. Q. Experimental investigation of a two-stage nonlinear vibration isolation system with high-static-low-dynamic stiffness. *Journal of Applied Mechanics-Transactions of the ASME*, **84**, 021001 (2017)

[2] XUE, J. R., ZHANG, Y. W., DING, H., and CHEN, L. Q. Vibration reduction evaluation of a linear system with a nonlinear energy sink under harmonic and random excitation. *Applied Mathematics and Mechanics* (*English Edition*), **41**(1), 1–14 (2020) https://doi.org/10.1007/s10483-020-2560-6

[3] QU, Y. G., XIE, F. T., and MENG, G. Nonlinear dynamic and acoustic analysis of orthogonally stiffened composite laminated cylindrical shells containing piecewise isolators. *Journal of Sound and Vibration*, **456**, 199–220 (2019)

[4] LU, Z. Q., BRENNAN, M., DING, H., and CHEN, L. Q. High-static-low-dynamic-stiffness vibration isolation enhanced by damping nonlinearity. *Science China Technological Sciences*, **62**, 1103–1110 (2019)

[5] MORADPOUR, S. and DEHESTANI, M. Optimal DDBD procedure for designing steel structures with nonlinear fluid viscous dampers. *Structures*, **22**, 154–174 (2019)

[6] CHEN, X. Q., SHEN, Z. P., HE, Q. S., DU, Q., and LIU, X. E. Influence of uncertainty and excitation amplitude on the vibration characteristics of rubber isolators. *Journal of Sound and Vibration*, **377**, 216–225 (2016)

[7] LU, Z. Q., HU, G. S., DING, H., and CHEN, L. Q. Jump-based estimation for nonlinear stiffness and damping parameters. *Journal of Vibration and Control*, **25**, 325–335 (2019)

[8] TANG, B. and BRENNAN, M. J. A comparison of two nonlinear damping mechanisms in a vibration isolator. *Journal of Sound and Vibration*, **332**, 510–520 (2013)

[9] HO, C., LANG, Z. Q., and BILLINGS, S. A. A frequency domain analysis of the effects of nonlinear damping on the Duffing equation. *Mechanical Systems and Signal Processing*, **45**, 49–67 (2014)

[10] YANG, J., XIONG, Y. P., and XING, J. T. Vibration power flow and force transmission behaviour of a nonlinear isolator mounted on a nonlinear base. *International Journal of Mechanical Sciences*, **115**, 238–252 (2016)

[11] LV, Q. B. and YAO, Z. Y. Analysis of the effects of nonlinear viscous damping on vibration isolator. *Nonlinear Dynamics*, **79**, 2325–2332 (2015)

[12] HUANG, X. C., SUN, J. Y., HUA, H. X., and ZHANG, Z. Y. The isolation performance of vibration systems with general velocity-displacement-dependent nonlinear damping under base excitation: numerical and experimental study. *Nonlinear Dynamics*, **85**, 777–796 (2016)

[13] BREWICK, P. T., MARSI, S. F., CARBONI, B., and LACARBONARA, W. Data-based nonlinear identification and constitutive modeling of hysteresis in nitinol and steel strands. *Journal of Engineering Mechanics*, **142**, 04016107 (2016)

[14] ZHAO, Z. W., WU, J. J., LIANG, B., LIU, H. Q., and SUN, Q. W. Numerical investigations on mechanical behavior of friction damped post-tensioned steel connections. *Archive of Applied Mechanics*, **88**, 2247–2260 (2018)

[15] FOTI, F., MARTINELLI, L., and PEROTTI, F. A new approach to the definition of self-damping for stranded cables. *Meccanica*, **51**, 2827–2845 (2016)

[16] AMJADIAN, M. and AGRAWAL, A. K. Modeling, design, and testing of a proof-of-concept prototype damper with friction and eddy current damping effects. *Journal of Sound and Vibration*, **413**, 225–249 (2018)

[17] GU, X. Y., YU, Y., LI, Y. C., LI, J. C., ASKARI, M., and SAMALI, B. Experimental study of semi-active magnetorheological elastomer base isolation system using optimal neuro fuzzy logic control. *Mechanical Systems and Signal Processing*, **119**, 380–398 (2019)

[18] KIANI, M. and VASEGHI-AMIRI, J. Effects of hysteretic damping on the seismic performance of tuned mass dampers. *Structural Design of Tall and Special Buildings*, **28**, e1555 (2019)

[19] ZHANG, Y. W., XU, K. F., ZANG, J., NI, Z. Y., ZHU, Y. P., and CHEN, L. Q. Dynamic design of a nonlinear energy sink with NiTiNOL-steel wire ropes based on nonlinear output frequency response functions. *Applied Mathematics and Mechanics* (*English Edition*), **40**(12), 1791–1804 (2019) https://doi.org/10.1007/s10483-019-2548-9

[20] MARKOU, A. A. and MANOLIS, G. D. Mechanical formulations for bilinear and trilinear hysteretic models used in base isolators. *Bulletin of Earthquake Engineering*, **14**, 3591–3611 (2016)

[21] SAUTER, D. and HAGEDORN, P. On the hysteresis of wire cables in Stockbridge dampers. *International Journal of Non-Linear Mechanics*, **37**, 1453–1459 (2002)

[22] CASINI, P. and VESTRONI, F. Nonlinear resonances of hysteretic oscillators. *Acta Mechanica*, **229**, 939–952 (2018)

[23] BARBIERI, N., BARBIERI, R., SILVA, R. A., MANNALA, M. J., and BARBIERI, L. S. V. Nonlinear dynamic analysis of wire-rope isolator and Stockbridge damper. *Nonlinear Dynamics*, **86**, 501–512 (2016)

[24] CARBONI, W. and LACARBONARA, W. Nonlinear vibration absorber with pinched hysteresis: theory and experiments. *Journal of Engineering Mechanics*, **142**, 04016023 (2016)

[25] SOLOVYOV, A. M., SEMENOV, M. E., MELESHENKO, P. A., and BARSUKOV, A. I. Bouc-Wen model of hysteretic damping. *Procedia Engineering*, **201**, 549–555 (2017)

[26] LIU, T., BRISEGHELLA, B., ZHANG, Q. L., and ZORDAN, T. Equivalent damping of bilinear hysteretic SDOF system considering the influence of initial elastic damping. *Soil Dynamics and Earthquake Engineering*, **97**, 74–85 (2017)

[27] CHEN, L. Q., LI, X., LU, Z. Q., ZHANG, Y. W., and DING, H. Dynamic effects of weights on vibration reduction by a nonlinear energy sink moving vertically. *Journal of Sound and Vibration*, **451**, 99–119 (2019)

[28] CHEN, Y. Y., YAN, L. W., SZE, K., Y., and CHEN, S. H. Generalized hyperbolic perturbation method for homoclinic solutions of strongly nonlinear autonomous systems. *Applied Mathematics and Mechanics* (*English Edition*), **33**(9), 1137–1152 (2012) https://doi.org/10.1007/s10483-012-1611-6

[29] ZHANG, Y. W., LU, Y. N., ZHANG, W., TENG, Y. Y., YANG, H. X., YANG, T. Z., and CHEN, L. Q. Nonlinear energy sink with inerter. *Mechanical Systems and Signal Processing*, **125**, 52–64 (2019)

[30] JIANG, W. N., ZHANG, G. C., and CHEN, L. Q. Forced response of quadratic nonlinear oscillator: comparison of various approaches. *Applied Mathematics and Mechanics* (*English Edition*), **36**(11), 1403–1416 (2015) https://doi.org/10.1007/s10483-015-1991-7

[31] XIONG, H., KONG, X. R., LI, H. Q., and YANG, Z. G. Vibration analysis of nonlinear systems with the bilinear hysteretic oscillator by using incremental harmonic balance method. *Communications in Nonlinear Science and Numerical Simulation*, **42**, 437–450 (2017)

[32] WU, R. P., BAI, H. B., and LU, C. H. Simplified analysis of hysteresis dry friction vibration isolation system on flexible foundation (in Chinese). *Journal of Mechanical Strength*, **41**, 44–48 (2019)

[33] WONG, C. W., NI, Y. Q., and LAU, S. L. Steady-state oscillation of hysteretic differential model, I: response analysis. *Journal of Engineering Mechanics*, **120**, 2271–2298 (1994)

[34] YUAN, T. C., YANG, J., and CHEN, L. Q. A harmonic balance approach with alternating frequency/time domain progress for piezoelectric mechanical systems. *Mechanical Systems and Signal Processing*, **120**, 274–289 (2019)

[35] ZHANG, Z. Y. and CHEN, Y. S. Harmonic balance method with alternating frequency/time domain technique for nonlinear dynamic system with fractional exponential. *Applied Mathematics and Mechanics* (*English Edition*), **35**(4), 423–436 (2014) https://doi.org/10.1007/s10483-014-1802-9

[36] IKHOUANE, F., EURTADO, J. E., and RODELLAR, J. Variation of the hysteresis loop with the Bouc-Wen model parameters. *Nonlinear Dynamics*, **48**, 361–380 (2007)